

ON THE STRUCTURE AND PROPERTIES OF DIFFERENTIALLY ROTATING, MAIN-SEQUENCE STARS IN THE 1 – 2 M_{\odot} RANGE

K. B. MACGREGOR, STEPHEN JACKSON, ANDREW SKUMANICH, T. S. METCALFE

*High Altitude Observatory, NCAR, P. O. Box 3000, Boulder, CO 80307**

Astrophysical Journal, Accepted

ABSTRACT

We conduct a systematic examination of the properties of models for chemically homogeneous, differentially rotating, main-sequence stars of mass 1 – 2 M_{\odot} . The models were constructed using a code based on a reformulation of the self-consistent field method of computing the equilibrium stellar structure for a specified conservative internal rotation law. The code has recently been upgraded with the addition of new opacity, equation of state, and energy generation routines, and a mixing-length treatment of convection in the outer layers of the stellar interior. Relative to nonrotating stars of the same mass, these models all have reduced luminosities and effective temperatures, and flattened photospheric shapes (i.e., decreased polar radii) with equatorial radii that can be larger or smaller, depending on the degree of differential rotation. For a fixed ratio of the axial rotation rate to the surface equatorial rotation rate, increasingly rapid rotation generally deepens convective envelopes, shrinks convective cores, and can lead to the presence of a convective core (envelope) in a 1 M_{\odot} (2 M_{\odot}) model, a feature that is absent in a nonrotating star of the same mass. The positions of differentially rotating models for a given mass M in the H-R diagram can be shifted in such a way as to approximate the nonrotating ZAMS over ranges in luminosity and effective temperature that correspond to a mass interval between M and about 0.7 M . We briefly note a few of the implications of these results, including (i) possible ambiguities arising from similarities between the properties of rotating and nonrotating models of different masses, (ii) a reduced radiative luminosity for a young, rapidly rotating Sun, (iii) the nuclear destruction of lithium and other light metallic species in the layers beneath an outer convective envelope, and (iv), the excitation of solar-like oscillations and the operation of a solar-like hydromagnetic dynamo in some 1.5 – 2 M_{\odot} stars.

Subject headings: stars: interiors — stars: rotation

1. INTRODUCTION

Rotation is a universal stellar physical attribute. This conclusion is supported by an enormous body of observational data, accrued over a period of nearly 100 years, from which information about rotational speeds and periods, the dependence of these quantities on parameters such as mass and age (i.e., evolutionary state), and the effects of rotation on the shape, effective temperature, chemical homogeneity, and other basic properties of stars have been inferred. Despite increasing evidence that rotation can have a significant impact on a variety of stellar characteristics, it is generally not included as a component of the structural/evolutionary models which are the primary tools for the interpretation of observations. This omission is, in part, a consequence of the increased complexity of the problem of determining the structure and evolution of a rapidly, differentially rotating star: a one-dimensional model necessarily becomes two-dimensional, the gravitational potential must be derived by solution of Poisson's equation, and the uncertain physics of convective and circulatory flows, along with other rotation-dependent mechanisms that contribute to angular momentum redistribution and chemical mixing, needs to be addressed.

Some progress toward the development of a straightforward yet robust technique for computing the internal structure of a rotating star has recently been made with the implementation of a new version of the self-consistent field (SCF) method (Jackson, MacGregor, & Skumanich 2005, hereafter Paper I). In its original form (Ostriker & Mark 1968; see also Jackson 1970), the SCF approach to computing a model for an

assumed conservative law of rotation consisted of two separate steps: (i) determination of the gravitational potential for a given distribution of the mass density ρ , followed by (ii) solution of the equations of stellar structure with the potential from (i) to update the equilibrium distributions of ρ and other quantities. The process was initiated with a trial distribution for ρ , and the two steps were executed sequentially and iterated upon until the densities from (i) and (ii) agreed to within a specified tolerance. While the SCF method was successfully used to construct detailed models of rotating upper-main-sequence stars (Bodenheimer 1971), it failed to converge for objects less massive than about 9 M_{\odot} , behavior which precluded its application to intermediate- and low-mass stars (see, e.g., Chambers 1976; Clement 1978, 1979; Paper I).

As described in Paper I (see also §2 below), the reformulated SCF method circumvents the difficulties responsible for nonconvergence in lower-mass, more centrally condensed stars with an approach that entails the specification of trial functions for the pressure P , the temperature T , and the shape of constant-density surfaces, together with iterative adjustment of both the profiles and central values of P and T . With these modifications, the method is capable of producing self-consistent models for rotating main-sequence stars of all masses. It has been validated through detailed comparisons with stellar models (both rotating and nonrotating) for masses $\geq 2 M_{\odot}$ computed by other investigators using alternative techniques (Paper I), and has been applied in an examination of the photospheric shape of the Be star Achernar, an object revealed by interferometric observations as highly flattened by rapid rotation (Jackson, MacGregor, & Skumanich 2004, and references therein). More recently, the structure

*The National Center for Atmospheric Research (NCAR) is sponsored by the National Science Foundation.

code based on the method has undergone considerable renovation, with the replacement of routines for the equation of state, nuclear energy generation rates, and opacities, and the addition of a mixing length treatment of convection. It is now equipped for use in an investigation of the effects of rotation on the structure and properties of stars with masses $\leq 2 M_{\odot}$.

In the present paper, we use the formalism described above to conduct a detailed survey of the structural characteristics of differentially rotating stars having masses M in the range $1 \leq M \leq 2 M_{\odot}$. In the absence of rotation, this mass interval encompasses considerable variation in internal properties, with the gross structure of objects at the lower limit consisting of an inner radiative core and an outer convective envelope, changing to a convective core and radiative envelope for objects at the upper limit. The influence of rotation on the basic morphology of stellar interiors for these masses has not received much attention, with rotation-related effects usually treated as perturbations to the nonrotating structure, if at all (see, e.g., Thompson et al. 2003). However, observations indicate the occurrence of surface rotation speeds rapid enough to imply non-negligible modifications to many stellar properties, particularly if the rotation is differential: the projected rotation speeds of $2 M_{\odot}$ main-sequence stars are typically in excess of 100 km s^{-1} , and comparable values have been measured for near zero-age main-sequence (ZAMS) $1 M_{\odot}$ stars in young clusters (Stauffer 1991; Wolff & Simon 1997; Tassoul 2000, and references therein).

Motivated by these considerations, we have constructed an extensive set of self-consistent models for $1 - 2 M_{\odot}$ ZAMS stars, to systematically study the dependence of stellar characteristics on the rate and degree of differential rotation. Our SCF models extend previous computational results for stars in this mass range, some of which were obtained for uniformly rotating configurations (Faulkner, Roxburgh, & Strittmatter 1968; Sackmann 1970; Kippenhahn & Thomas 1970; Papaloizou & Whelan 1973; Roxburgh 2004), while others were obtained using either approximate methods for nonconservative differential rotation (Endal & Sofia 1981; Pinsonneault et al. 1989; Eggenberger, Maeder, & Meynet 2005) or a non-SCF, finite-difference technique in the case of conservative rotation (Clement 1979). In §2 we provide a synopsis of the new SCF method, briefly describing its implementation in a code for computing the structure of chemically homogeneous, differentially rotating main sequence stars, the improvements and extensions to the input physics that have been made since Paper I, and the results of tests of code reliability through comparisons with extant models for nonrotating ZAMS stars with masses $\leq 2 M_{\odot}$. An examination of the properties of models spanning a wide range of internal rotation characteristics is presented in §3, with particular attention paid to the behavior of such quantities as luminosity and effective temperature, central thermodynamic properties, the location and extent of convective regions, and the size and shape of the stellar photosphere. Among the consequences of these rotation-induced changes in stellar properties is a shift in the position of objects in the classical H-R diagram (HRD); indeed, for some adopted rotation laws, the resulting structural modifications can enable a differentially rotating star to have the same T_{eff} and L values as a non-rotating star of significantly lower mass and to thereby occupy the same position in the HRD. In the concluding section of the paper (§4), we use the model results to consider how the changes brought on by rapid differential rotation might affect other features of main-sequence stars in this mass range, such as the radiative lumi-

osity of the young Sun and associated effects on the planets, the abundance of lithium in the surface layers of mid-F dwarf stars, and the presence of strong, large-scale magnetic fields in some A stars.

2. THE NEW SCF METHOD

2.1. Implementation

The new version of the SCF method (described in detail in Paper I) is an iterative scheme that is initialized by specifying (i) a pair of one-dimensional trial functions, one for the temperature distribution and one for the pressure distribution (each normalized by its central value and defined over a spatial range that is normalized by the equatorial radius of the star), and (ii) a two-dimensional normalized function describing the shape of the equidensity surfaces. The normalized two-dimensional trial density distribution, which is used as the source term in Poisson's equation for the gravitational potential, follows from the equation of state and the trial functions for P and T . For a conservative law of rotation, in which the angular velocity depends only on the perpendicular distance from the axis of rotation, it is possible to define an effective potential from which both the gravitational and centrifugal forces can be derived. The surfaces of constant effective potential (i.e., level surfaces) can then be identified and used to solve a set of ordinary differential equations analogous to the usual equations of stellar structure for nonrotating stars. This solution step yields updated temperature and pressure distributions, allowing the iterative cycle to be repeated and the process continued until convergence is achieved. When the input and output functions representing the normalized temperature and pressure profiles are in agreement, the two parameters corresponding to the central temperature (T_c) and central pressure (P_c) are adjusted by a Newton-Raphson technique to bring them closer to the actual physical conditions at the center of the final equilibrium model. The entire procedure (consisting of an SCF loop nested inside a Newton-Raphson loop) is repeated until an acceptable level of agreement between the input and output values of the two central parameters is attained. When used to construct models for differentially rotating main-sequence stars, this reformulation of the SCF method has been shown to converge for all masses in the range $0.6 \leq M \leq 30 M_{\odot}$, and for values of the dimensionless rotational kinetic energy t (the ratio of the rotational kinetic energy to the absolute value of the gravitational potential energy of the configuration) as high as 0.10–0.12 for intermediate- and high-mass models, and up to nearly 0.26 for some fully convective, highly flattened, disk-like, $1 M_{\odot}$ models. By comparison, the largest t values among the non-SCF models computed by Clement (1978, 1979) were ≈ 0.18 for $30 M_{\odot}$ and ≤ 0.12 for models in the range $1.5 \leq M \leq 5 M_{\odot}$, whereas Bodenheimer (1971) obtained a $60 M_{\odot}$ SCF model with $t \approx 0.24$.

As in Paper I (see also Jackson, MacGregor, & Skumanich 2004), the internal rotation of each of the stellar models discussed in §3 is given by an angular velocity distribution of the form

$$\Omega(\varpi) = \frac{\Omega_0}{1 + (\alpha\varpi/R_e)^2}, \quad (1)$$

where $\varpi = r \sin \theta$, and R_e is the equatorial radius of the star. For a given model, the constants Ω_0 and α are prescribed parameters that characterize, respectively, the axial rotation rate and the ratio of the surface equatorial rotation rate to the axial rate (a measure of the degree of differential rotation),

$\Omega_e/\Omega_0 = 1/(1+\alpha^2)$. In practice, the value of the first of these quantities is specified through the parameter $\eta = \Omega_0/\Omega_{cr}$, with Ω_{cr} the equatorial angular velocity for which the magnitudes of the gravitational and centrifugal forces at R_e are equal.

Rigorous answers to questions about the existence and uniqueness of solutions to complicated systems of integro-differential equations are generally very difficult to obtain. Although specifying the two rotational parameters α and η for chemically homogeneous models of fixed mass and composition does not always lead to a converged model, when it does, our experience with the code suggests that the model is unique. For a given set of (α, η) values, using the SCF code to converge models of the same mass and chemical composition from two or more *different* trial models always seems to lead to the *same* final converged model. On the other hand, it can be demonstrated that specifying the parameters α and Ω_0 does not, in general, lead to a unique solution. A minor drawback to use of the parameters (α, η) in presenting the results is that several important global properties, including the luminosity L , the total angular momentum J , and the dimensionless rotational kinetic energy t , are not monotonic functions of η when α is held fixed (see also §3.1). Despite this shortcoming, we feel that the apparent uniqueness of the models corresponding to particular (α, η) values justifies the use of these quantities in presenting and discussing results. We emphasize that sequences of models obtained by holding α fixed and varying η should not be interpreted as any sort of evolutionary sequence. The significance of models characterized by the same value of α is that they have the same degree of differential rotation, that is, the same Ω_e/Ω_0 . The “half-width” of the rotation profile, $\varpi_{1/2} = R_e/\alpha$, does, however, change from model to model for constant α .

2.2. Input Physics

Since the publication of Paper I, the input physics for the SCF code described therein has been updated considerably, with the installation of software components that at various times were parts of the stellar-evolution code developed by Don Vandenberg at the University of Victoria. All of the models presented in this paper were computed for the following abundances by weight of H, He, and heavy elements: $X = 0.7112$, $Y = 0.27$, and $Z = 0.0188$. The opacities were obtained, as in Vandenberg et al. (2000), from tables of OPAL opacities calculated by Rogers & Iglesias (1992) and from tables of low-temperature opacities calculated by Alexander & Ferguson (1994), using interpolation subroutines written by Vandenberg (1983). Other subroutines written by Vandenberg (1992) were utilized for the following: (i) the equation of state formulated by Eggleton, Faulkner, & Flannery (1973, EFF); (ii) nuclear energy generation rates for hydrogen burning from Caughlan & Fowler (1988), including the effect of electron screening as treated by Graboske et al. (1973) for the case of equilibrium abundances of CNO isotopes; and (iii) a standard mixing-length treatment of surface convective zones (see, e.g., Baker & Temesvary 1966; Kippenhahn, Weigert, & Hofmeister 1967). We have made no attempt to incorporate any of the direct effects of rotation into the adopted convection model; instead, we have simply modified the nonrotating mixing-length description of convection by replacing the local gravitational acceleration, \mathbf{g} , with the effective gravitational acceleration, $\mathbf{g}_{eff} = \mathbf{g} - \Omega(\varpi)^2 \mathbf{e}_\varpi$ (i.e., \mathbf{g} as reduced by the local centrifugal acceleration), averaged over equipotential surfaces. For all of the models, a value of 1.9 for the ratio of the mixing length to the pressure scale height has been

adopted.

2.3. Validation

In view of the revisions and updates that have been made to the SCF code of Paper I, it seems worthwhile to make a careful comparison of our nonrotating models for stars on the lower main sequence with models for the same mass obtained from a standard (nonrotating) stellar evolution code. For this purpose, we have used the current version of the evolutionary code of Christensen-Dalsgaard (1982, hereafter referred to as the JCD code) to generate two evenly spaced sequences of seven models each, spanning the mass range $0.8 \leq M \leq 2.0 M_\odot$ along the ZAMS. These models have chemical composition $X = 0.711$, $Z = 0.019$, quite close to the abundances adopted for our SCF models, and were computed using the same value (1.9) of the mixing length parameter. The basic EFF equation of state was used to construct one of the sequences, while the other was derived with the so-called CEFF equation of state, a modification of the EFF treatment that includes Coulomb corrections (see, e.g., Christensen-Dalsgaard & Dappen 1992). Aside from the inclusion or omission of Coulomb effects in the equation of state, the package of input-physics routines used to generate the JCD models is very similar to that installed in the SCF code (see, e.g., Christensen-Dalsgaard, Proffitt, & Thompson 1993; Di Mauro & Christensen-Dalsgaard 2001). In addition to the intrinsic distinctions between the mathematical techniques used to obtain the two sets of models, the current version of the SCF code differs from the JCD code in the following ways: (i) the equation of state does not include treatment of Coulomb corrections; (ii) the photospheric pressure in the SCF code follows from the application of a different, simplified boundary condition (see Paper I); and (iii), there is a slight difference in the vintage of the nuclear energy generation data.

We have conducted a quantitative comparison of some of the important properties (R , L , T_{eff} , P_c , T_c , ρ_c) of SCF, JCD/EFF, and JCD/CEFF models for nonrotating ZAMS stars of the same mass. A theoretical HRD indicating the positions of the various models is displayed in Figure 1. The EFF and CEFF main sequences (the dashed and dotted lines, respectively) are very nearly coincident, with the former models shifted along the locus relative to the latter models, toward somewhat lower luminosities and effective temperatures. On the basis of the preceding discussion, we expect the SCF models to agree better with EFF models than with CEFF models, and inspection of the results plotted in Figure 1 indicate that this is generally the case. For the luminosity, the most sensitive of the stellar properties, the largest discrepancies occur for the $0.8 M_\odot$ models, with the SCF L about 2% lower than that of the EFF model of the same mass; this latter value is, in turn, about 7% lower than L for the corresponding CEFF model. The luminosities of the SCF and EFF models are essentially equal for $2 M_\odot$, while a comparison of the EFF and CEFF models for that mass reveals that the CEFF model is about 3% more luminous. The effective temperatures and radii of the SCF models deviate from those of the corresponding EFF models by less than 1%, except for those models between 1.2 and $1.4 M_\odot$ where the magnitudes of the discrepancies are somewhat larger, $\approx 1\% - 2\%$. The SCF values for P_c and ρ_c differ from the EFF values of those quantities by about 2%, with the relative difference in the T_c values $\lesssim 1\%$. There is also good qualitative agreement between the SCF and JCD models with respect to the appearance or ab-

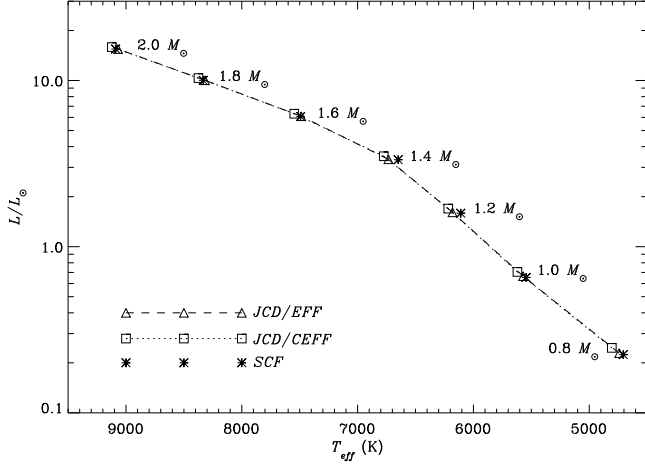


FIG. 1.— A theoretical HR diagram showing the positions of nonrotating, chemically homogeneous stellar models for the indicated masses, as computed using different codes and equations of state. The various symbols denote models obtained using the SCF code of the present paper (*), a current version of the code of Christensen-Dalsgaard (1982, JCD) with the simplified equation of state of Eggleton, Faulkner, & Flannery (1973, EFF) (Δ), and the JCD code with a version of the EFF equation of state that includes Coulomb corrections (CEFF) (\square). The dashed and dotted lines are the computed ZAMS locations derived from the JCD/EFF and JCD/CEFF models, respectively.

sence of convective cores and envelopes, and there is good quantitative agreement with respect to the radial extent and the enclosed mass of the principal radiative-convective interfaces.

3. PROPERTIES OF DIFFERENTIALLY ROTATING STELLAR MODELS

3.1. Convergence Properties

The properties of SCF models for rotating ZAMS stars with masses $1 \leq M \leq 2 M_\odot$ are summarized in Figures 2-8 and Table 1. To facilitate discussion of the computed stellar characteristics, we adopt the convention, established in Paper I, of identifying each model by its mass, M , and the two rotational parameters, α and η , for the reasons discussed in §2. Regions of the (α, η) parameter space in which converged $6 M_\odot$ SCF models can and cannot be obtained have been illustrated in Figure 3 of Paper I. While the (α, η) planes for the lower-mass SCF models considered here closely resemble that for the $6 M_\odot$ models, there are some important differences. Of particular relevance to the present paper are the regions corresponding to Region II in Paper I, regions of relatively high angular momentum wherein the SCF method is incapable of producing converged models. These *forbidden zones* are considerably expanded for the 1 and $2 M_\odot$ models: for the former models, the values (α_t, η_t) corresponding to the lower tip of this region are $\alpha_t = 1.39$, $\eta_t \approx 2.4$, while for the latter, $\alpha_t = 2.83$ and $\eta_t \approx 6.5$. Along each constant- α sequence for $0 < \alpha < \alpha_t$, quantities such as the axial angular velocity Ω_0 and the total angular momentum J are non-monotonic functions of η , increasing to a maximum for $\eta \approx \eta_t$ and decreasing thereafter. As $\alpha \rightarrow \alpha_t$, convergence in the vicinity of this maximum becomes significantly slower, and fails completely when α is large enough (i.e., $> \alpha_t$) to place the model within the forbidden zone. For $\alpha_t < \alpha \leq 7$ (the largest value of α we have considered), converged models can be readily obtained on the low- η sides of these regions. On the high- η sides, converged models can be obtained only within the ranges

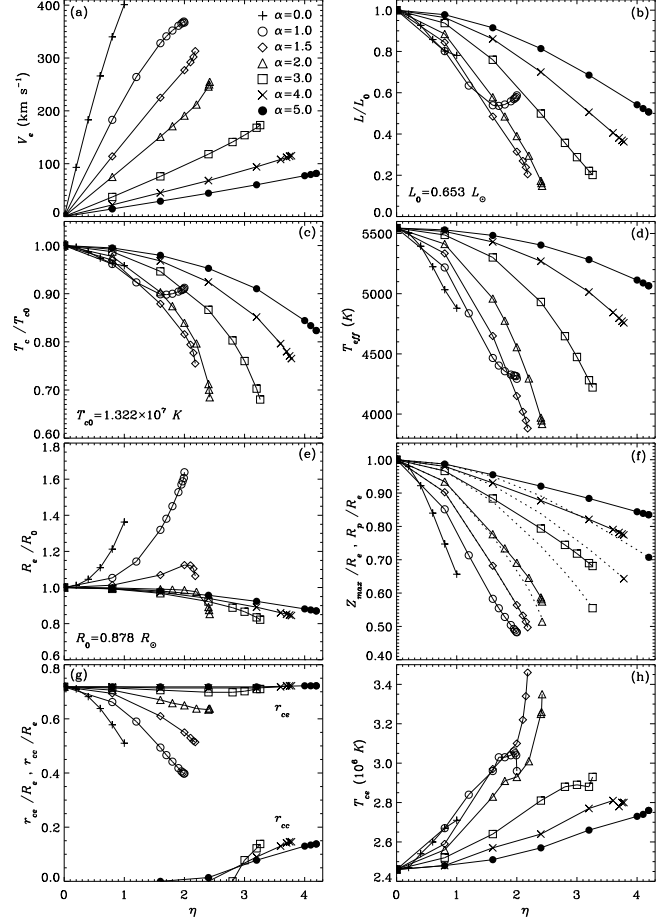


FIG. 2.— Selected properties of differentially rotating, $1 M_\odot$, ZAMS stellar models. The model characteristics are shown as functions of η for $0 \leq \alpha \leq 5$, where the parameters α and η specify the assumed internal angular velocity distribution given by equation (1). The quantities depicted in the various panels include: (a) the surface equatorial rotation speed V_e ; (b) the luminosity L in units of L_0 , the luminosity of a nonrotating $1 M_\odot$ model; (c) the central temperature T_c relative to the corresponding value T_{c0} for the nonrotating model; (d) the average effective temperature T_{eff} ; (e) the equatorial radius R_e in units of R_0 , the radius of the nonrotating model; (f) the maximum perpendicular distance Z_{max} from the equatorial plane to the photosphere (solid curves), and the polar radius R_p (dotted curves), as fractions of R_e ; (g) the radii of the base of the convective envelope r_{ce} and the convective core r_{cc} , both measured in the equatorial plane relative to R_e ; and, (h) the temperature T_{ce} at the base of the convective envelope.

$1.39 \leq \alpha \leq 3$ for the $1 M_\odot$ models, and $2.83 \leq \alpha \leq 3.47$ for the $2 M_\odot$ models. The physical, mathematical, and computational reasons for the lack of convergence of models on either side of the forbidden zone are discussed in considerable detail in Paper I. In this paper, we present results for complete constant- α sequences of models having $\alpha < \alpha_t$, but confine our attention to just the low- η sides of forbidden zones for models with $\alpha > \alpha_t$. Models on the high- η sides of these regions have highly rotationally flattened, disk-like structures that will be the focus of a subsequent paper.

3.2. $1 M_\odot$ Models

In Figure 2, we show how some of the characteristics of the $1 M_\odot$ models depend on the dimensionless rotation parameter η for $0 \leq \alpha \leq 5$. The relation between η and the physical quantity V_e , the equatorial rotation speed at the stellar surface, is given in panel (a), from which it can be seen that for each

TABLE 1. SELECTED MODELS

Model	I	II	III	IV	V	VI	VII	VIII	IX	X	XI
M	0.8	1	1	1	1	1.2	1.2	1.6	2	2	2
α	0	0	1.5	3.75	5	0	4	0	0	3	4.75
η	0	0	1.55	3.58	4.15	0	3.74	0	0	5.64	5.9
t	0	0	0.044	0.079	0.052	0	0.065	0	0	0.047	0.078
J	0	0	6.44	7.27	5.49	0	8.93	0	0	23.71	23.73
V_e	0	0	219	123	81	0	112	0	0	205	127
L	0.224	0.653	0.332	0.224	0.336	1.591	0.653	6.075	15.47	7.560	6.083
T_{eff}	4710	5540	4710	4700	5080	6110	5550	7490	9090	5890	7480
$\log g_s$	4.635	4.551	4.478	4.709	4.679	4.412	4.616	4.310	4.337	3.855	4.404
R_e	0.714	0.878	0.934	0.744	0.767	1.129	0.904	1.466	1.590	2.927	1.512
R_p/R_e	1	1	0.697	0.638	0.712	1	0.668	1	1	0.371	0.549
Z_{max}/R_e	1	1	0.697	0.764	0.837	1	0.791	1	1	0.530	0.770
$\log P_c$	17.078	17.178	17.100	16.967	17.019	17.259	17.101	17.326	17.287	17.317	17.282
$\log T_c$	7.046	7.121	7.069	7.004	7.039	7.187	7.094	7.280	7.326	7.289	7.255
$\log \rho_c$	1.892	1.918	1.893	1.823	1.841	1.935	1.869	1.911	1.827	1.893	1.892
$\rho_c/\bar{\rho}$	25	40	35	17	20	73	29	114	96	446	83
r_{cc}/R_e	0.138	0.138	0.046	0.090	0.094	0.122	0.054	0.110
m_{cc}/M	0.023	0.031	0.007	0.014	0.082	0.141	0.085	0.074
r_{ce}/R_e	0.678	0.718	0.618	0.718	0.722	0.822	0.746	0.990	0.990	0.718	...
m_{ce}/M	0.921	0.968	0.905	0.935	0.950	0.997	0.972	1.000	1.000	0.995	...
$\log T_{ce}$	6.458	6.392	6.467	6.452	6.440	6.104	6.388	4.780	4.771	5.988	...
Fig.	3a	3b	3c	...	3d	3e	3f

NOTE. — Quantities listed (units in parentheses): total mass, M (M_\odot); rotational parameters, α , η ; dimensionless rotational kinetic energy, t ; total angular momentum, J (10^{50} g cm² s⁻¹); equatorial velocity, V_e (km s⁻¹); luminosity, L (L_\odot); mean effective temperature, T_{eff} (K); mean surface gravity, g_s (cm s⁻²); equatorial radius, R_e (R_\odot); polar radius, R_p ; maximum (normal) distance from the equatorial plane to the surface of star, Z_{max} ; central pressure, P_c (dyn cm⁻²); central temperature, T_c (K); central density, ρ_c (g cm⁻³); mean density, $\bar{\rho}$; distance in the equatorial plane from the center to the top of the convective core, r_{cc} , and to the bottom of the convective envelope, r_{ce} ; mass enclosed by the upper bounding surface of the convective core, m_{cc} , and by the lower bounding surface of the convective envelope, m_{ce} ; and temperature at the bottom of the convective envelope, T_{ce} (K).

of the α sequences depicted, V_e increases monotonically with η . Along the curves with $\alpha < \alpha_t$ in Figure 2, the plotted models span the range from $\eta = 0$ (i.e., nonrotating) to the value $\eta = 1 + \alpha^2$ for which $\Omega_e = \Omega_{cr}$. Along the curves with $\alpha > \alpha_t$, the last plotted model is located adjacent to the boundary of the forbidden region in the (α, η) plane; for these differentially rotating models, the centrifugal and gravitational forces have nearly equal magnitudes in the core of the star. We note that the degree of differential rotation increases with α , in the sense that the configurations corresponding to larger values of α have a greater difference between the axial and surface equatorial rates of rotation (see §2.1).

As panel (b) of Figure 2 makes evident, the radiative luminosities of these models are diminished relative to the luminosity L_0 of a nonrotating $1 M_\odot$ star. This is a well-known consequence of including rotation in the determination of the equilibrium stellar structure (see, e.g., Clement 1979; Bodenheimer 1971). In the results shown in Figure 2, the reduction in L is larger for differentially rotating models than it is for models that are uniformly or nearly uniformly rotating. A model with $\alpha = 0$ rotating at the break-up rate ($\eta = 1$) has $L/L_0 = 0.78$, while an $\alpha = 2$ model with $\eta = 2.42$ has $L/L_0 = 0.15$, a reduction of more than a factor of 6 from the nonrotating value. Much of the reason for this behavior lies in the effect of rotation on the thermodynamic conditions in the deep, energy-producing regions of the stellar interior. For these $1 M_\odot$ models, the contribution of the centrifugal force to supporting material against gravity enables the star to emulate an object of lower mass with correspondingly reduced values of P_c , T_c , and ρ_c (e.g., Sackmann 1970). The results presented in panel (c) illustrate the dependence of T_c on model rota-

tional properties; similar variations are found for both P_c and ρ_c . For rigidly rotating configurations, this centrifugal support is largest in the outermost layers of the interior, which contain only a small fraction of the stellar mass; in this case, P_c , T_c , and ρ_c are little changed from the values appropriate to a nonrotating star of the same mass. For the $\alpha = 0$, $\eta = 1$ model noted previously, $P_c/P_{c0} = 0.94$, $T_c/T_{c0} = 0.96$, and $\rho_c/\rho_{c0} = 0.98$, where the subscript 0 indicates the nonrotating value. Alternatively, in models for higher values of α , the effects of rotation are increasingly concentrated toward the central regions of the star, with the result that the perturbations to the central thermodynamic quantities can be more substantial; for $\alpha = 2$, $\eta = 2.42$, $P_c/P_{c0} = 0.56$, $T_c/T_{c0} = 0.68$, and $\rho_c/\rho_{c0} = 0.81$. Panels (b) and (c) also indicate that the magnitudes of the changes in L , T_c , and other quantities depend on the assumed profile of internal differential rotation. The model for $\alpha = 5$, $\eta = 4$ has $L/L_0 = 0.54$, with $P_c/P_{c0} = 0.72$, $T_c/T_{c0} = 0.84$, and $\rho_c/\rho_{c0} = 0.85$, smaller reductions relative to the nonrotating model than those for $\alpha = 2$, $\eta = 2.42$. This behavior is an outgrowth of the structural modifications arising from the centrifugal force distributions associated with the different rotation profiles. In the $\alpha = 5$ model, the ratio of the centrifugal to gravitational force in the equatorial plane, $\Omega^2 r/g$ (r is the radial coordinate in the equatorial plane), is sharply peaked in the innermost portion of the stellar core, with maximum value 0.83 at the center, decreasing to ≈ 0.1 at $r/R_e = 0.3$. For the shallower angular velocity profile of the $\alpha = 2$ model, the force ratio decreases from a smaller central value of 0.42 to 0.23 at the stellar surface, 10 times the value found throughout the outer 50% of the interior of the $\alpha = 5$ model.

In this connection, we note that Bodenheimer (1971) found that the luminosities of models for rotating $30 M_{\odot}$ stars, computed assuming a variety of internal rotation laws, depended primarily on the total angular momentum content of a given stellar model and not on the details of its distribution within the interior. Specifically, his results indicated that the luminosities of models corresponding to four different prescribed distributions of the angular momentum per unit mass decreased with increasing total angular momentum J , with the relation between L and J nearly the same for each model sequence. If the luminosities of our $1 M_{\odot}$ models are plotted versus their respective J values, an analogous reduction in L for increasing J can be discerned. However, the relation between L and J is roughly independent of α only for small J , and exhibits a clear dependence on α that becomes increasingly pronounced as J is made larger. That the luminosity can be even approximately expressed as a function of J necessarily reflects the modifications produced by rotation to the thermodynamic conditions in the energy-producing core of the star, as described previously (see also Mark 1968). The nature and origin of the relation between L and J for stars with masses $1 - 2 M_{\odot}$ and higher, including its dependence on the structural characteristics of the models, will be addressed in detail in a subsequent paper in this series.

As in Paper I, we define an average effective temperature through the relation $T_{eff} = (L/\sigma A)^{1/4}$, where σ is the Stefan-Boltzmann constant and A the area of the stellar surface. The results for T_{eff} depicted in panel (d) exhibit dependences on α and η that are similar to those seen for the quantities plotted in the preceding panels. Reductions by more than $1500 K$ from the nonrotating value ($T_{eff} = 5540 K$) are possible as, for example, in the case $\alpha = 1.5$, $\eta = 2.18$, for which $T_{eff} = 3880 K$. The rotation-induced variations in T_{eff} represent the combined effects of changes in both L and A . An indication as to the behavior of A can be gleaned from examination of the influence of rotation on the stellar size and shape. This information is presented in panels (e) and (f), where we show, respectively, the equatorial radius R_e (in units of the radius R_0 of the nonrotating, spherical $1 M_{\odot}$ model), and the polar radius R_p together with Z_{max} , the maximum perpendicular distance from the equatorial plane to the stellar surface. These latter two quantities are both given as fractions of R_e ; values of R_p/R_e that are < 1 reflect a rotational flattening of the configuration, while values of Z_{max}/R_e that are $\neq R_p/R_e$ are indicative of a deviation from a convex spheroidal shape through the development of a concavity in each of the two polar regions of the star.

Note that the response of the equatorial radius to increasing η differs greatly depending upon whether α is $\lesssim 1.5$ or $\gtrsim 2$. In the former case, the centrifugal force attains its largest value relative to the gravitational force at the stellar surface, consequently producing a distension of the outer, equatorial layers of the stellar interior and an overall increase in R_e . Although R_p decreases somewhat relative to the radius of the corresponding nonrotating model, the net effect of the changes in R_e and R_p is usually an increase in the volume of the rotating star. For some models with $\alpha \approx \alpha_t$, the decrease in R_p can more than compensate for the increase in R_e , and the volume of the rotating star is reduced. In the case where $\alpha \gtrsim 2$, both R_e and the stellar volume shrink with increasing η along a constant- α sequence. For these models, the centrifugal force is largest in comparison to the gravitational force in the central region of the stellar core, causing the central thermodynamic

conditions, luminosity, and size (i.e., radius, surface area, volume) to assume values that are characteristic of nonrotating stars of lower mass. This raises the possibility that a differentially rotating star can imitate a less massive nonrotating star in radius and effective temperature, as well as in luminosity. In panel (f), it can be seen that for $\alpha \lesssim 1.5$, the curves for Z_{max}/R_e (solid lines) and R_p/R_e (dotted lines) are coincident and < 1 , implying that the photospheric shape of these models is oblate spheroidal. Such a model ($\alpha = 1.5$, $\eta = 1.55$) is depicted in panel (a) of Figure 3. For $\alpha > 2$, however, $Z_{max} > R_p$, symptomatic of the development of a “dimple” or indentation at either pole, as in the cases of the models shown in panels (b) ($\alpha = 3.75$, $\eta = 3.58$) and (c) ($\alpha = 5$, $\eta = 4.15$) of Figure 3.

Panels (g) and (h) of Figure 2 contain results pertaining to the location, extent, and properties of convective regions in the models. In the absence of rotation, the internal structure of a $1 M_{\odot}$ star consists of an inner, radiative core that encompasses $\approx 72\%$ of the stellar radius and contains $\approx 97\%$ of the stellar mass, surrounded by an outer, convective envelope. As is apparent in panel (g), the inclusion of rotational effects can modify this basic morphological picture in two ways: either by increasing the size of the convective envelope or by promoting the formation of a convective core.

For lower values of α (i.e., $\alpha < 3$ in panel [g]), the rotationally induced changes in internal structure cause the outer convection zone to deepen as η increases. For example, in the model with $\alpha = 1.5$, $\eta = 1.55$ (see panel [a] in Figure 3), the radius in the equatorial plane of the base of the convective envelope is $r_{ce}/R_e = 0.618$, significantly deeper than the base radius $r_{ce}/R_e = 0.718$ in the nonrotating model. Associated with this reduction in r_{ce} is a decrease in the mass of the core ($m_c/M \approx 0.90$), and an increase in the temperature T_{ce} at the bottom of the envelope, as can be seen in panel (h); for the $\alpha = 1.5$, $\eta = 1.55$ model, $T_{ce} = 2.93 \times 10^6 K$, as compared with $T_{ce} = 2.46 \times 10^6 K$ for the nonrotating model. Since some chemical species (e.g., Li, Be, and B) can be destroyed by thermonuclear reactions at temperatures $\gtrsim 2.5 \times 10^6 K$, enhancements of T_{ce} of this magnitude are likely to have consequences for the surface abundances of these elements. In the case of the strongly differentially rotating models with $\alpha \geq 3$, the largest centrifugal effects are concentrated in the innermost portion of the core, so that the fractional thickness of the outer envelope is little affected. However, as the magnitude of the centrifugal-to-gravitational force ratio in the core increases for larger η , the decreasing pressure gradient implied by the requirement of hydrostatic equilibrium forces the otherwise stably stratified central regions of the interior to become convective. Under these conditions, with the presence of a convective core, the structure of the deep interior resembles that of a higher-mass star. The models shown in panels (b) and (c) of Figure 3 are examples of $1 M_{\odot}$ stars with convective cores; in each of these models, the radial extent of this region in the equatorial plane is about 14% of R_e and contains $\approx 2 - 3\%$ of the stellar mass. For comparison, the convective core in a model for a nonrotating $2 M_{\odot}$ star has a radius that is about 12% of R_e and contains $\approx 14\%$ of the stellar mass.

To illustrate the structural differences between differentially and near-uniformly rotating stars, in Figure 4 we show the profiles of several physical quantities for models with $(\alpha, \eta) = (3.00, 3.26)$, and $(1.00, 1.20)$, along with the corresponding results for the nonrotating model. The luminosities and total angular momenta of the two rotating models are $L/L_0 = 0.201$ and $J = 9.23$ ($\alpha = 3$), and $L/L_0 = 0.634$ and $J = 5.30$ ($\alpha = 1$), respectively, where J is measured in units

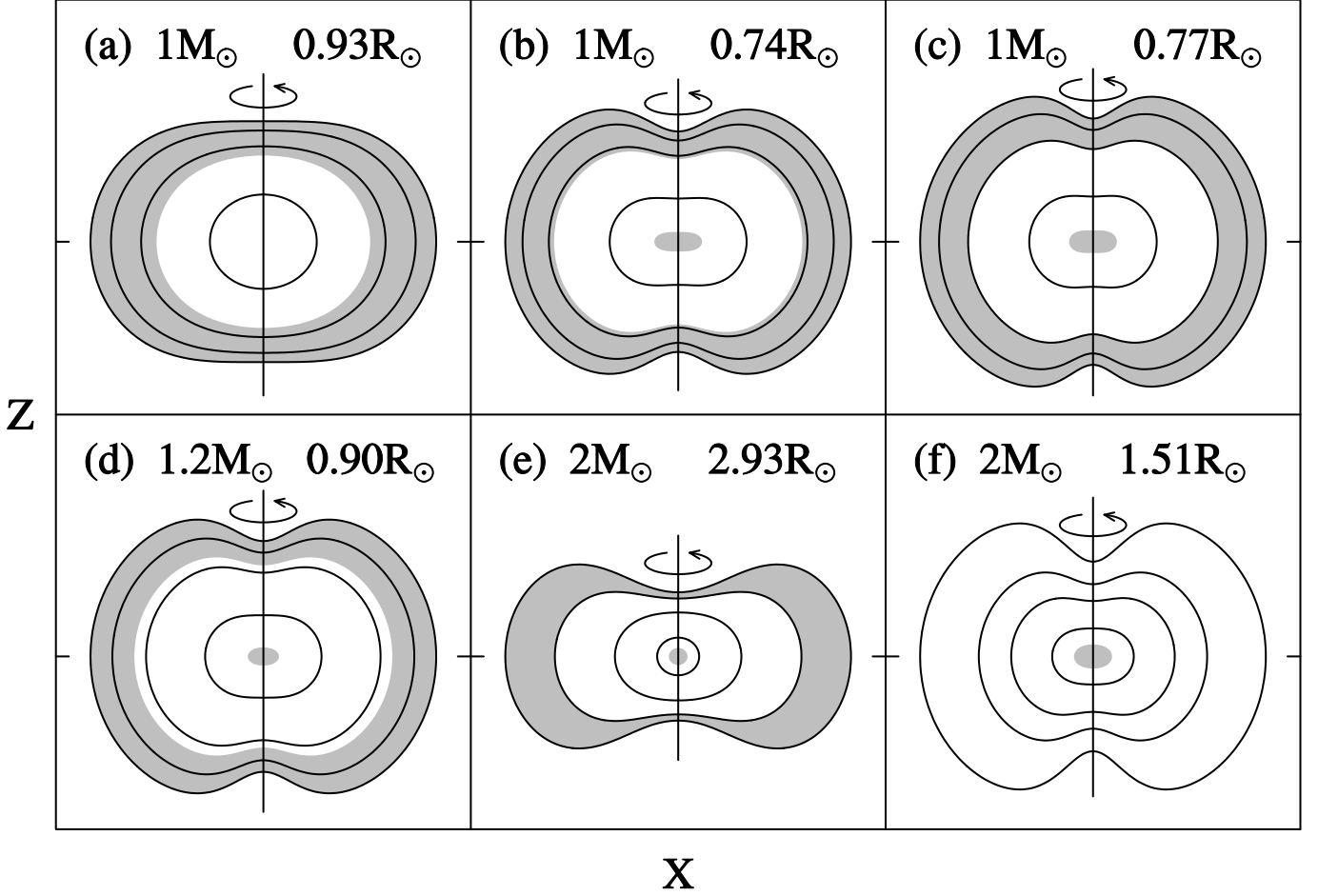


FIG. 3.— Contours of level surfaces in the meridional plane for some of the nonspherical models listed in Table 1. The six rotating models shown are defined by the total mass and the two rotational parameters (M , α , η) as follows: (a) $1 M_{\odot}$, 1.5, 1.55; (b) $1 M_{\odot}$, 3.75, 3.58; (c) $1 M_{\odot}$, 5, 4.15; (d) $1.2 M_{\odot}$, 4, 3.74; (e) $2 M_{\odot}$, 3, 5.64; and, (f) $2 M_{\odot}$, 4.75, 5.9. From the surface inward, the level surfaces depicted in each panel enclose a fraction of the total mass equal to 1.000, 0.995, 0.950, and 0.500, respectively. The fractional radii in the equatorial plane of these level surfaces for the various models are: (a) 1.00, 0.88, 0.71, 0.31; (b) 1.00, 0.90, 0.75, 0.40; (c) 1.00, 0.89, 0.72, 0.37; (d) 1.00, 0.87, 0.68, 0.34; (e) 1.00, 0.71, 0.37, 0.12; and, (f) 1.00, 0.66, 0.47, 0.24. Radiative portions of the interior are indicated in white, and convective regions are shaded gray. The fractional equatorial radii and enclosed masses for the interfaces between radiative and convective zones in the models are listed in Table 1. The numbers at the tops of the panels denote the total mass M and equatorial radius R_e of each model.

of $10^{50} \text{ g cm}^2 \text{ s}^{-1}$. In panels (a) and (b), the temperature T and mass density ρ are depicted as functions of the radial position r (measured in units of the present-day solar radius R_{\odot}) in the equatorial plane of the star. The central values of both quantities exhibit rotation-induced reductions relative to the nonrotating case, the magnitudes of these modifications being larger for $\alpha = 3$ ($T_c/T_{c0} = 0.68$, $\rho_c/\rho_{c0} = 0.76$) than for $\alpha = 1$ ($T_c/T_{c0} = 0.92$, $\rho_c/\rho_{c0} = 0.97$). As noted previously, this behavior is a consequence of differences in the magnitudes and distributions of the centrifugal force in the two rotating models. These distinctions can be clearly seen in the profiles of the centrifugal-to-gravitational force ratio shown in panel (d). For $\alpha = 3$, the force ratio is largest in the deep interior, attaining a maximum value of 0.96 at the stellar center and decreasing outwards to a magnitude ≈ 0.1 in the photosphere. For $\alpha = 1$, the ratio increases monotonically throughout the interior, rising from a central value of just 0.026 to a maximum of 0.36 at R_e . The substantial contribution of the centrifugal force to the support of the innermost regions of the $\alpha = 3$ model is responsible for the considerable enhancement of the density scale height there, evident in panel (b); ρ declines by only $\approx 10\%$ over the inner 20% of the stellar interior. The resulting changes in the internal mass distribution (panel [c])

lead to a star with a smaller radius, $R_e = 0.72 R_{\odot}$ as opposed to $R_e = 0.88 R_{\odot}$ for the nonrotating model. Alternatively, for the $\alpha = 1$ model, the lack of centrifugal support in the core of the star leads to temperature, density and mass distributions therein that closely resemble those of the nonrotating model. Closer to the surface, however, the density distribution becomes extended, a product of the increasing centrifugal reduction of gravity in the outer layers of the interior; as a result, the stellar radius is larger than that of the nonrotating model, $R_e = 1.00 R_{\odot}$.

3.3. Solar Look-Alike Models

Figure 5 is a theoretical HRD for $1 M_{\odot}$ models that span a broad range of internal rotational states, from uniform rotation to extreme differential rotation (up to $\Omega_0 = 50 \Omega_e$ for $\alpha = 7$). The nonrotating ZAMS is delineated by a dotted line, with the positions of several specific models for $0.6 \leq M \leq 1.0 M_{\odot}$ indicated. Clearly, as already implied by panels (b) and (c) of Figure 2, the locations of rotating models in such a diagram are displaced to the right of and below the position they would occupy in the absence of rotation, toward lower values of both the luminosity and the effective temperature. Models with uniform or near-uniform internal rotation (i.e., $\alpha = 0, 1$) lie

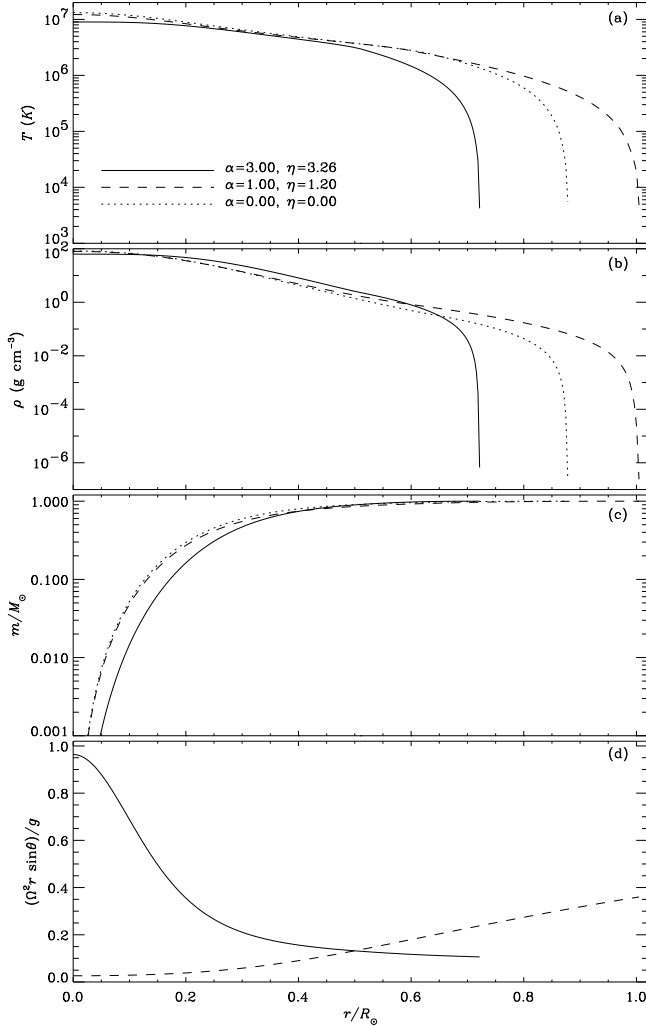


FIG. 4.— Profiles of selected physical quantities in the interiors of $1 M_{\odot}$ models with $(\alpha, \eta) = (3.00, 3.26)$ (solid curves), $(1.00, 1.20)$ (dashed curves), and $(0.00, 0.00)$ (dotted curves). The profiles depict the dependence of each quantity on radial position r in the equatorial plane, from the center of the star to the surface. The various panels show (a) the temperature T , (b) the mass density ρ , (c) the fraction m/M of the total mass contained within a level surface that intersects the equatorial plane at r , and (d) the ratio $(\Omega^2 r \sin \theta)/g$ of the centrifugal force to the gravitational force.

well above the nonrotating ZAMS, while those for which the degree of differential rotation is substantial ($\alpha \geq 3$) have positions in the HRD that collectively approximate the nonrotating ZAMS over virtually the entire mass range depicted. For example, the rotating $1 M_{\odot}$ model ($\alpha = 3.75$, $\eta = 3.58$) shown in panel (b) of Figure 3 is characterized by $T_{\text{eff}} = 4700 \text{ K}$ and $L/L_{\odot} = 0.224$, which is indistinguishable from the values $T_{\text{eff}} = 4710 \text{ K}$, $L/L_{\odot} = 0.224$ for a nonrotating, $0.8 M_{\odot}$ model. Such a coincidence of the positions of stars of different mass in the classical HRD is made possible by the fact that the largest structural changes take place in the cores of strongly differentially rotating models. Specifically, the decrease in L brought about by the smaller values of P_c , T_c , and ρ_c , together with the corresponding reduction in R_e , enable such a model to effectively mimic a lower mass stellar model in which rotational effects are not included.

Figure 6 illustrates some of the internal properties of three so-called *solar look-alike* models, that is, models for differ-

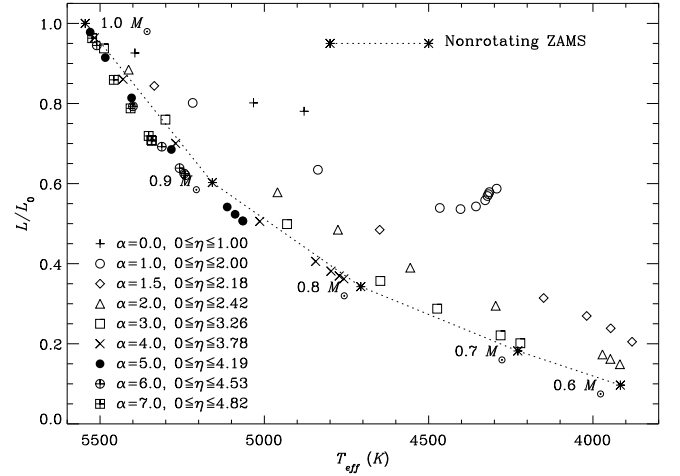


FIG. 5.— A theoretical HR diagram showing the positions of models for rotating, ZAMS, $1 M_{\odot}$ stars. Luminosities are given in units of the luminosity $L_0 = 0.653 L_{\odot}$ of a non-rotating, $1 M_{\odot}$ star. The various symbols denote models constructed using the rotation law of equation (1) with the values of the parameters (α, η) listed in the Figure. The ZAMS for non-rotating stars is indicated by the dotted line, with the positions of models for masses 0.6, 0.7, 0.8, 0.9, and 1.0 along it marked by an * symbol.

entially rotating stars with masses $> 1 M_{\odot}$ that have many physical attributes in common with the model for a nonrotating, $1 M_{\odot}$ star. Inspection of panels (a) and (b) reveals that the profiles and the central values of the temperature and density for the 1.1, 1.2, and $1.3 M_{\odot}$ models depicted therein are quite close to those of the solar-mass model with $\alpha = \eta = 0$. A consequence of these structural similarities is that many of the general characteristics of the models are nearly identical. For example, the $1.2 M_{\odot}$ model which, in the absence of rotation, would have $L/L_{\odot} = 1.591$, $R_e/R_{\odot} = 1.129$, and $T_{\text{eff}} = 6110 \text{ K}$ instead has $L/L_{\odot} = 0.653$, $R_e/R_{\odot} = 0.904$, and $T_{\text{eff}} = 5546 \text{ K}$, compared with $L/L_{\odot} = 0.653$, $R_e/R_{\odot} = 0.878$, and $T_{\text{eff}} = 5545 \text{ K}$ for the nonrotating, $1 M_{\odot}$ model. A cross-section in the meridional plane of the rotating $1.2 M_{\odot}$ interior is shown in panel (d) of Figure 3, from which it can be seen that a solar-like convection zone having $r_{ce}/R_e = 0.746$ is present in the layers beneath the photosphere. With a surface equatorial rotation speed $V_e = 112 \text{ km s}^{-1}$, such an object could be mistakenly identified as a rapidly rotating $1 M_{\odot}$ star, if observations were analyzed through comparison with non-rotating stellar models. *That the values of measureable or inferable stellar properties can be the same in rotating and nonrotating models for different masses represents a potential source of ambiguity in the interpretation of a variety of observations.* Panels (c) and (d) reveal subtle differences in the internal mass distributions and in the variation of the ratios of the centrifugal to gravitational force in the equatorial planes of these solar look-alike models. Future space-based asteroseismological observations may be capable of exploiting such differences in internal structure to distinguish slowly rotating stars from more rapidly, differentially rotating higher-mass stars that happen to have the same values of L and T_{eff} and thus occupy the same position in the HRD (see, e.g., Lochar et al. 2005).

3.4. $2 M_{\odot}$ Models

In Figure 7, we present a summary of the rotational dependence of $2 M_{\odot}$ model characteristics, using the same format as adopted for Figure 2. The model for a non-rotating star of this

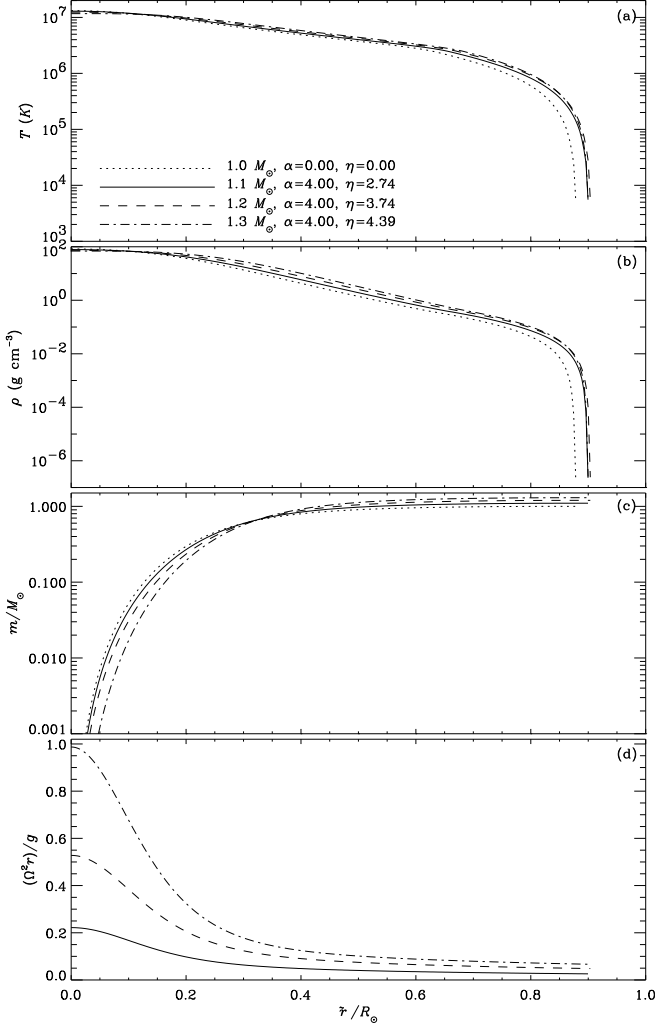


FIG. 6.— Profiles in the equatorial plane of the temperature (a), density (b), mass fraction (c), and the ratio of the centrifugal to gravitational acceleration (d) for a nonrotating, $1 M_\odot$ model ($\alpha = \eta = 0$) and three solar look-alike models. The latter models were obtained for $(M, \alpha, \eta) = (1.1 M_\odot, 4.00, 2.74)$, $(1.2 M_\odot, 4.00, 3.74)$ and $(1.3 M_\odot, 4.00, 4.39)$, and have values of T_{eff} and L that differ from those of the non-rotating, solar model by about 1% or less.

mass has $L_0 = 15.47 L_\odot$, $R_0 = 1.59 R_\odot$, and $T_{\text{eff}} = 9090 K$, and a convective core with $r_{\text{cc}}/R_e = 0.122$, $m_{\text{cc}}/M = 0.141$; such a model has a thin, subsurface convective layer, $r_{\text{ce}}/R_e = 0.99$, that contains a negligible fraction of the stellar mass. The results shown in Figure 7, which span the rotational parameter ranges $0 \leq \alpha \leq 5$, $0 \leq \eta \leq 7$, exhibit many of the same behaviors as noted previously in connection with the $1 M_\odot$ models of Figure 2. In particular, along each constant- α sequence, the luminosity (panel [b]), central temperature, (panel [c]) and effective temperature (panel [d]) all initially decrease as η is increased, with the largest reductions in these quantities occurring in the cases of differentially rotating models with $\alpha \geq 3$. For $\alpha = 1, 2$, both L/L_0 and T_c/T_{c0} pass through minima and then increase slightly with η beyond those points, whereas T_{eff} continues to decrease with η for all α sequences. The central pressure P_c (panel [e]), on the other hand, is an increasing function of η for $0 \leq \alpha \leq 3$, and displays a non-monotonic dependence on η for the model sequences corresponding to $\alpha = 4, 5$. The origin of this variation is the mass dependence

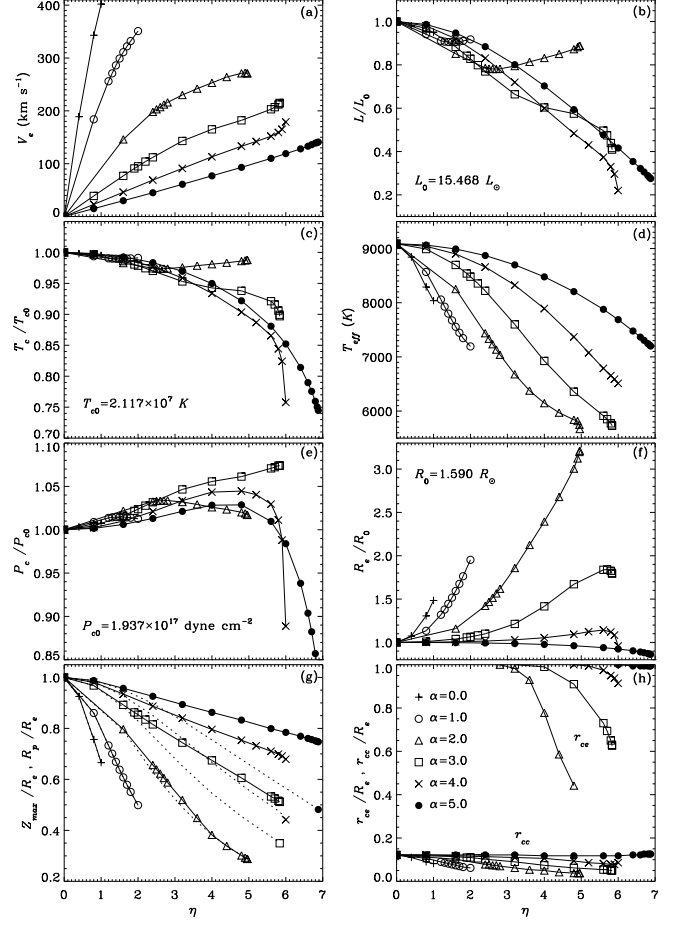


FIG. 7.— Selected properties of differentially rotating, $2 M_\odot$, ZAMS stellar models, as in Figure 2. The quantities depicted in the various panels include: (a) V_e , (b) L , (c) T_c , (d) T_{eff} , (e) P_c , (f) R_e , (g) Z_{max} and R_p , and (h) r_{cc} and r_{ce} .

of P_c for stars on the non-rotating ZAMS. In our SCF models without rotation, P_c has a maximum value for M near $1.6 M_\odot$, and is decreasing for both larger and smaller M values. The maximum occurs for a mass close to the value marking the internal structural transition between stars with radiative cores and convective envelopes and stars with convective cores and radiative envelopes. Hence, insofar as the properties of a rotating star are like those of a non-rotating star of lower mass, we expect the P_c values of these $2 M_\odot$ models to increase as the effects of rotation become more pronounced. For cases in which the central thermodynamic conditions are significantly perturbed by rapid, differential rotation in the core of the star, this mass-lowering effect can be large enough to shift P_c to values characteristic of nonrotating stars with $M < 1.6 M_\odot$ (i.e., on the other side of the central pressure peak), as in the $2 M_\odot$ models for $\alpha = 4, 5$.

Panels (f) and (g) of Figure 7 convey information pertaining to the photospheric sizes and shapes of the models. Those that rotate nearly rigidly are equatorially distended, and, in the direction perpendicular to the equatorial plane, have their largest dimension along the rotation axis ($Z_{\text{max}} = R_p$); since $R_p < R_e$, these models (like their $1 M_\odot$ counterparts) have a flattened, spheroidal shape. Models with increasing degrees of differential rotation (i.e., with $\alpha \gtrsim 3$) develop polar concavities (as indicated by $Z_{\text{max}} > R_p$), and ultimately (i.e., for

$\alpha = 4, 5$ and sufficiently large η) become more compact, with $R_e < R_0$. Panels (e) and (f) of Figure 3 give cross-sectional representations of the photospheric shapes of $2 M_\odot$ models for $(\alpha, \eta) = (3.00, 5.64)$ and $(4.75, 5.90)$, respectively; in the former model, $R_e = 2.93 R_\odot > R_0$, while for the latter, $R_e = 1.51 R_\odot < R_0$.

The influence of rotation on the occurrence and extent of convective regions within the models is explored in panel (h) of Figure 7. The convective core, a salient feature of the non-rotating stellar interior, generally decreases in size as the value of η is increased. This contraction stems from a reduction in the magnitude of the radiative gradient ∇_{rad} in the core region of the star, a result of the way in which the central thermodynamic conditions are modified by rotation (see, e.g., MacGregor & Gilliland 1986); with ∇_{rad} smaller, the size of the region wherein it exceeds the adiabatic gradient ∇_{ad} shrinks accordingly. Only for the most rapidly, differentially rotating models does r_{cc} show a modest increase compared to the non-rotating model; in panel [h], the model for $(\alpha, \eta) = (5.00, 6.88)$ has $r_{cc}/R_e = 0.124$. In this case, as was seen for the $1 M_\odot$ models having convective cores in Figure 2, the growth of r_{cc} can be traced to a *larger* value of ∇_{rad} , produced by a centrifugal-to-gravitational force ratio that is nearly unity at the stellar center. Note also that for some $2 M_\odot$ models, the convection zone underlying the stellar photosphere can extend into the stellar interior by more than the few $10^{-3} R_0$ that is the thickness of this region in the absence of rotation. As can be seen, for example, in panel (e) of Figure 3, the base of the convective envelope in the equatorial plane of the model with $(\alpha, \eta) = (3.00, 5.64)$ is located at $r_{ce}/R_e = 0.718$, a fractional depth which is the same as in the non-rotating $1 M_\odot$ model. This leads to the intriguing possibility that solar-like oscillations, driven by turbulent convection, may be excited in stars that would normally be too massive to generate them. The results shown in panel (h) suggest that such a solar-like convective envelope is most likely to occur in $2 M_\odot$ models with intermediate differential rotation (say., $\alpha \approx \alpha_t = 2.83$). For a profile of this kind, the inner and outer portions of the interior can each rotate rapidly enough to both significantly perturb the thermodynamic conditions in the core and increase R_e by extending the stellar envelope.

In Figure 8, we show the positions of models for differentially rotating, $2 M_\odot$ stars in a theoretical HRD. As in Figure 5, the location of the non-rotating ZAMS is indicated by a dotted line, with the positions of models for stars with masses in the range $1.0 \leq M \leq 2.0 M_\odot$ indicated along it. This HRD for rotating $2 M_\odot$ models has a number of features in common with the corresponding representation of $1 M_\odot$ properties. Without exception, models are shifted from the non-rotating location to new positions characterized by lower T_{eff} and L values. For $\alpha \lesssim 3$, these new positions lie to the right-hand side of (i.e., above) the non-rotating ZAMS; for rotation that is increasingly differential, however, the model locations approach the non-rotating ZAMS, moving just to the left-hand side of (i.e., below) it for $\alpha = 5$. For $\alpha = 4.75$, the model positions are distributed along the non-rotating ZAMS, delineating its track in the HRD for masses greater than about $1.5 M_\odot$. This coincidence again raises the possibility that a rapidly, differentially rotating $2 M_\odot$ star could effectively masquerade as a non-rotating star of lower mass. As an example, with $L/L_\odot = 6.083$, $R_e/R_\odot = 1.512$, and $T_{eff} = 7480 K$ the model for $(\alpha, \eta) = (4.75, 5.90)$ shown in panel (f) of Figure 3 closely resembles a non-rotating $1.6 M_\odot$ star, for which $L/L_\odot = 6.075$, $R_e/R_\odot = 1.466$, and $T_{eff} = 7490 K$.

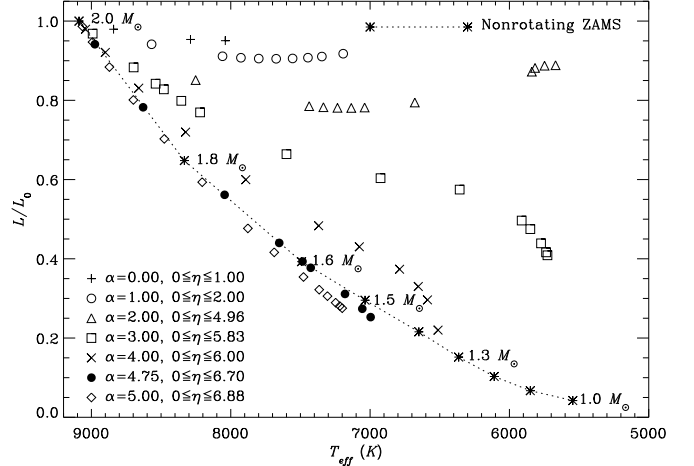


FIG. 8.— A theoretical HR diagram showing the positions of models for rotating, $2 M_\odot$ ZAMS stars, as in Figure 5. Luminosities are given in units of the luminosity $L_0 = 15.468 L_\odot$ of a nonrotating, $2 M_\odot$ star. The ZAMS for nonrotating stars is indicated by the dotted line, with the positions of models for masses $1.0, 1.1, 1.2, 1.3, 1.4, 1.5, 1.6, 1.8$, and $2.0 M_\odot$ along it marked by an * symbol.

4. SUMMARY AND DISCUSSION

The SCF approach to computing the structure of rotating stars is robust and efficient, capable of yielding converged models of stars of all masses, with internal angular-velocity distributions covering the range from uniform to extreme differential rotation. The code described in Paper I has been upgraded through the introduction of opacities, energy generation rates, and an equation of state that are close to state-of-the-art, and with the introduction of a mixing-length treatment of convective energy transport. We have used this revised code to conduct a systematic study of the properties of models for rotating ZAMS stars with masses $1 \leq M \leq 2 M_\odot$, assuming that the rotation of the stellar interior can be adequately represented by the parameterized angular-velocity profile given in equation (1).

Our results suggest that rotation affects virtually every characteristic of the intermediate- and low-mass stars considered herein, with the magnitude, and sometimes even the sense, of the changes in fundamental attributes depending on both the rate and degree of the differential rotation in the stellar interior. For models that are uniformly or nearly uniformly rotating, the centrifugal contribution to the hydrostatic support of the star is largest in the outer layers of the interior; for models that are strongly differentially rotating, the centrifugal force is largest compared to gravity in the core of the star. Luminosities and effective temperatures are always diminished relative to nonrotating stars of the same mass, while equatorial radii increase in uniformly rotating or moderately differentially rotating models, and decrease in models where the difference between the angular velocity at the center and that at the equator is sufficiently large. As the degree of differential rotation is increased, the photospheric shape of the star changes from a convex surface closely approximating a spheroid flattened along the rotation axis to a roughly oblate surface with deepening polar concavities; in such cases, the greatest perpendicular distance from the equatorial plane to the surface occurs away from the axis of rotation, and is always less than the equatorial radius of the star. In $1 M_\odot$ models, the effects of rotation can either increase the thickness of

the outer convective envelope, or contribute to the formation of a convective core. In rotating $2 M_{\odot}$ models, the size of the convective core is diminished relative to that found in the absence of rotation, and an extensive, solar-like convection zone can be present in the outer layers of what would otherwise be a stable radiative envelope.

The extent to which the results of these computations accurately depict the stellar structural modifications arising from rotation depends on the validity of a number of simplifying assumptions and approximations made in the course of developing the basic model, as well as on the inherent limitations of the SCF method itself. Here, we briefly address the most salient of the factors that might restrict the applicability of these results, noting where improvements and extensions can (or cannot) be made (see also Paper I).

1). The modified SCF iterative scheme utilized in the present investigation necessarily requires the angular velocity distribution within the star to be conservative, and thus expressible as a function of just the perpendicular distance from the rotation axis, $\Omega = \Omega(\varpi)$ (see eq. [1]). Although this specification facilitates the construction of models through the considerable mathematical simplification it introduces, its effect on some computed stellar structural characteristics, such as the photospheric shapes and core physical properties of very rapidly, differentially rotating models, is likely to differ from that produced by a rotation law of (say) the form $\Omega = \Omega(r)$. There is some evidence, from both simulations and observations, for the occurrence of differential rotation of the type given by equation (1) (see, e.g., Dobler, Stix, & Brandenburg 2006, and references therein). Yet analyses of solar acoustic oscillations yield a picture of the large-scale internal dynamics of the Sun which is not in accord with the angular velocity being constant on cylindrical surfaces (see Thompson et al. 2003). We note that use of the SCF method precludes consideration of non-conservative rotation laws (e.g., $\Omega = \Omega(r)$); however, detailed treatment of the hydrodynamical and magnetohydrodynamical processes affecting the internal rotational states of the Sun and stars is presently beyond the scope of *any* of the extant structural/evolutionary models.

2). The model treats only the prescribed rotational motion of the stellar interior, omitting any meridional circulatory flow and its consequent effects on the internal angular momentum distribution. For models with radiative envelopes, rotationally driven circulation will cause the rotation profile to deviate over time from the state given by equation (1), unless such evolution is mitigated by additional angular momentum transport mechanisms (see, e.g., Maeder & Meynet 2000, and references therein). For models with convective envelopes, the rotation profile in the outer layers of the interior is the product of the complex interplay between meridional circulation and turbulent heat and angular momentum transport (Rempel 2005; Miesch, Brun, & Toomre 2006); whether Ω is solar-like or constant on cylindrical surfaces depends on the latitudinal entropy distribution in the subadiabatically stratified layers below the convection zone.

3). The model employs a simplified treatment of convection, locating unstable regions by application of the Schwarzschild criterion and utilizing an averaged, rotationally modified mixing-length description (see §2.2) to determine the structure of an outer convective envelope, if present. Use of the Solberg-Høiland condition (e.g., Ledoux 1965; Kippenhahn & Weigert 1990) to ascertain the onset of convective instability would account for the direct influence of the centrifugal force. Since models computed for the rotation law of

equation (1) have $\partial j / \partial \varpi > 0$, where $j = \Omega \varpi^2$ is the specific angular momentum (see Paper I), this change would likely decrease the equatorial-plane thickness of an outer convection zone, and produce a latitudinal variation in r_{ce} . However, for rapid rotation, there is considerable uncertainty regardless of the convection criterion/model adopted, because of both the rudimentary nature of extant treatments of convective energy transport and the universal assumption of axisymmetry among rotating stellar models.

We reiterate that the present model describes a chemically homogeneous, ZAMS star, and neglects effects associated with the structural and compositional evolution of the stellar interior. We are presently developing a mean-field hydrodynamics-based treatment of turbulent chemical and angular momentum transport which maintains conservative rotation profiles, thus making it possible to investigate the main-sequence evolution of these SCF models. Despite the shortcomings enumerated above, we believe that the basic model and method described herein compare favorably with alternative approaches to determining the structure and evolution of rotating stars. The most widely used of these (e.g., Meynet & Maeder 1997) relies on the use of approximate, Roche-like equipotentials to represent the internal gravity of the star, thereby strictly limiting it to describing slowly rotating stars to ensure the accuracy of the computed models. Whatever its drawbacks, the SCF method yields two-dimensional, axisymmetric configurations that represent fully consistent solutions to both the set of stellar structure equations *and* Poisson's equation for the gravitational potential.

The results presented herein have a number of implications for young stars with masses between 1 and $2 M_{\odot}$. Measurements of projected equatorial rotation speeds in excess of 100 km s^{-1} for some solar-type stars in young open clusters (see, e.g., Stauffer 1991) raise the possibility that the structure and properties of these objects could be significantly altered from those of nonrotating stars of the same mass. Such stars, provided that their interior rotation is sufficiently differential, could in actuality be somewhat more massive objects for which surface rotation as rapid as that indicated by observations is the normally expected ZAMS state. The question of whether or not the kind of strong differential rotation required to produce such ambiguity is present within the interiors of some low- and intermediate-mass stars may ultimately be resolved through space-based asteroseismological observations, which should allow low-resolution inversions of the rotation profiles in the inner $\sim 30\%$ of the stellar radius (see Gough & Kosovichev 1993). Asteroseismology from space may also afford the means for identifying individual stars whose rotation enables them to pose as lower-mass objects, since, when effects associated with asphericity are not too large, the average mode frequency spacing is sensitive to the mean density, a quantity which Table 1 reveals to be different for *look-alike* models.

If rapid differential rotation is a possibility for objects in the mass range spanned by the models of §3, then the associated changes in structure and properties could have consequences for a variety of important astrophysical processes that take place within and around such stars. The reduced radiative luminosity of a rapidly rotating young Sun would likely influence the evolution of the solar nebula, and further exacerbate the discrepancies between the properties of nonrotating models and observational inferences indicating a higher ZAMS luminosity (see, e.g., Sackmann & Boothroyd 2003). The rotationally induced deepening of a sub-photospheric convection

zone, together with the increase in temperature of the material at the base, could contribute to the depletion of lithium in the stellar surface layers by reducing the thickness of the region through which chemical species must be transported in order to be destroyed by nuclear processes. The formation of a solar-like convective envelope in a young, differentially rotating, $2 M_{\odot}$ star could excite global oscillations, and be accompanied by the operation of a solar-like hydromagnetic dynamo. Dynamo-generated fields that diffuse into and are retained by the radiative interior (see, e.g., Dikpati, Gilman, & MacGregor 2006) could enable the star to remain magnetic long after spin-down and the elimination of nonuniform rotation have led to the disappearance of both the surface convec-

tive layer and the dynamo. Each of these possibilities will be addressed in forthcoming papers.

We wish to thank D. A. VandenBerg for providing software from his stellar-evolution code that was used to handle the input physics in our SCF code, and we wish to thank J. Christensen-Dalsgaard for the use of his stellar-evolution code to help us validate our models. This work was supported in part by an Astronomy & Astrophysics Postdoctoral Fellowship under award AST-0401441 (to T. S. M.) from the National Science Foundation.

REFERENCES

- Alexander, D. R., & Ferguson, J. W. 1994, *ApJ*, 437, 879
 Baker, N. H., & Temesvary, S. 1966, *Studies of Convective Stellar Envelopes* (NASA Goddard Inst. for Space Studies)
 Bodenheimer, P. 1971, *ApJ*, 167, 153
 Caughlan, G. R. & Fowler, W. A. 1988, *Atomic Data and Nuclear Data Tables*, 40, 283
 Chambers, R. H. 1976, Ph.D. thesis, University of Toronto
 Christensen-Dalsgaard, J. 1982, *MNRAS*, 199, 735
 Christensen-Dalsgaard, J., & Däppen, W. 1992, *A&A Review*, 4, 267
 Christensen-Dalsgaard, J., Proffitt, C. R., & Thompson, M. J. 1993, *ApJ*, 403, L75
 Clement, M. 1978, *ApJ*, 222, 967
 Clement, M. 1979, *ApJ*, 230, 230
 Dikpati, M., Gilman, P. A., & MacGregor, K. B. 2006, *ApJ*, 638, 564
 Di Mauro, M. P., & Christensen-Dalsgaard, J. 2001, in *Helio- and Asteroseismology at the Dawn of the Millenium*, Proc. of SOHO 10/GONG 2000 Workshop, ed. A. Wilson (Noordwijk: ESA), 373
 Dobler, W., Stix, M., & Brandenburg, A. 2006, *ApJ*, 638, 336
 Eggenberger, P., Maeder, A., & Meynet, G. 2005, *A&A*, 440, L9
 Eggleton, P. P., Faulkner, J., & Flannery, B. P. 1973, *A&A*, 23, 325
 Endal, A. S., & Sofia, S. 1981, *ApJ*, 243, 625
 Faulkner, J., Roxburgh, I. W., & Strittmatter, P. A. 1968, *ApJ*, 151, 203
 Gough, D. O., & Kosovichev, A. G. 1993, *ASP Conf. Ser.* 40: IAU Colloq. 137: Inside the Stars, 40, 541
 Graboske, H., DeWitt, H., Grossman, A., & Cooper, M. 1973, *ApJ*, 181, 457
 Jackson, S. 1970, *ApJ*, 161, 579
 Jackson, S., MacGregor, K. B., & Skumanich, A. 2004, *ApJ*, 606, 1196
 Jackson, S., MacGregor, K. B., & Skumanich, A. 2005, *ApJS*, 156, 245
 Kippenhahn, R., Weigert, A., & Hofmeister, E. 1967, *Meth. Comp. Phys.*, 7, 129
 Kippenhahn, R., & Thomas, H. -C. 1970, in *Stellar Rotation*, ed. A. Slettebak (New York: Gordon & Breach Pub.), 20
 Kippenhahn, R., & Weigert, A. 1990, *Stellar Structure and Evolution* (Berlin: Springer-Verlag)
 Ledoux, P. 1965, in *Stellar Structure*, eds. L. H. Aller & D. B. McLaughlin (Chicago: Univ. of Chicago Press), 499
 Lochard, J., Samadi, R., & Goupil, M. J. 2005, *A&A*, 438, 939
 MacGregor, K. B., & Gilliland, R. L. 1986 *ApJ*, 310, 273
 Maeder, A., & Meynet, G. 2000, *ARA&A*, 38, 143
 Mark, J. W. -K. 1968, *ApJ*, 154, 627
 Meynet, G., & Maeder, A. 1997, *A&A*, 321, 465
 Miesch, M. S., Brun, A. S., & Toomre, J. 2006, *ApJ*, 641, 618
 Ostriker, J. P., & Mark, J. W. -K. 1968, *ApJ*, 151, 1075
 Papaloizou, J. C. B., & Whelan, J. A. J. 1973, *MNRAS*, 164, 1
 Pinsonneault, M. H., Kawaler, S. D., Sofia, S., & Demarque, P. 1989, *ApJ*, 338, 424
 Rempel, M. 2005, *ApJ*, 622, 1320
 Rogers, F. J., & Iglesias, C. A. 1992, *ApJS*, 79, 507
 Roxburgh, I. W. 2004, *A&A*, 428, 171
 Sackmann, I. -J. 1970, *A&A*, 8, 76
 Sackmann, I. -J., & Boothroyd, A. I. 2003, *ApJ*, 583, 1024
 Stauffer, J. R. 1991, in *Angular Momentum Evolution of Young Stars*, ed. S. Catalano & J. R. Stauffer (Dordrecht: Kluwer Academic Pub.), 117
 Tassoul, J. -L. 2000, *Stellar Rotation* (Cambridge: Cambridge Univ. Press)
 Thompson, M. J., Christensen-Dalsgaard, J., Miesch, M. S., & Toomre, J. 2003, *ARA&A*, 41, 599
 VandenBerg, D. A. 1983, *ApJS*, 51, 29
 VandenBerg, D. A. 1992, *ApJ*, 391, 685
 VandenBerg, D. A., Swenson, F. J., Rogers, F. J., Iglesias, C. A., & Alexander, D. R. 2000, *ApJ*, 532, 430
 Wolff, S. C., & Simon, T. 1997, *PASP*, 109, 759